and DACHPt/m (4 mg/kg on a Pt base) on days 0, 2 and 4. Photon flux was measured until 2 weeks and was taken as a parameter of tumor volume. Body weight was measured simultaneously to assess the toxicity.

2.7. Antitumor activity against lymph node metastasis

To study the antitumor efficacy of the DACHPt/m against lymphatic metastasis, the mice were sacrificed at the end of the antitumor activity experiment and the metastatic lymph nodes were excised and weighed. The inhibition of the growth of the metastases was associated with the weight of the lymph nodes.

2.8. Accumulation of DACHPt/m in orthotopic tumors and metastatic lymph nodes

In order to analyze the biodistribution of oxaliplatin and DACHPt/m, OCUM-2MLN-Luc cells (5×10^6 cells/ml) were injected sub-serosally into the gastric walls of BALB/c nu/nu mice (female, $n=5$). Four weeks later, oxaliplatin and DACHPt/m were intravenously injected at a dose of 100 μg/mouse on a platinum basis. Mice were sacrificed after defined time periods (1, 4 and 24 h), and then tumor and metastatic lymph nodes were collected. Tissue samples were washed in ice-cold saline and weighed after removing excess fluid. All samples were dissolved in HNO_3 and evaporated to dryness. The Pt concentration was measured by ICP-MS after the samples were redissolved in 5N HCl.

2.9. Biodistribution of fluorescent-labeled DACHPt/m

DACHPt/m were labeled with Alexa 680 to investigate the accumulation in orthotopic gastric tumors and metastatic lymph nodes. OCUM-2MLN (5×10^6 cells/ml) cells were inoculated sub-serosally into the gastric walls of BALB/c nu/nu mice and the tumors were allowed to grow for about 3 weeks. Alexa 680-labeled DACHPt/m (5 mg/kg on Pt basis) were intravenously injected and the mice were imaged after 24 h to track the accumulation of micelles in the whole body by using IVIS imaging system (excitation: 640 nm; emission: 720 nm; exposure time: 1 s; field of view: 18.1 cm). Then, the mice were sacrificed and the organs (liver, kidney and spleen), the primary tumor and the metastatic lymph nodes were imaged *ex vivo* to evaluate the accumulation of micelles.

2.10. Microdistribution of fluorescent micelles in orthotopic tumor and lymph node metastasis

Tumor bearing mice were injected intravenously with Alexa 594-labeled DACHPt/m to evaluate their microdistribution in primary tumors and metastatic lymph nodes by histology. Tumors, metastatic and normal lymph nodes were excised, snapped frozen in liquid nitrogen and embedded in optimal cutting temperature compound (Tissue-Tek, Sakura Finetek). The frozen samples were sectioned at 10-μm thickness in a cryostat and fixed with 10% formalin. The tissue sections were stained with hematoxylin and eosin (H&E) and observed using an Olympus AX80 microscope (Olympus, Japan). For immunohistochemical analysis, the tissue sections were also stained for lymphatic vessels by using anti-LYVE-1 antibody (Abcam), blood vessels by using anti-PECAM-1 antibody (BD PharMingen), and cancer cells by using anti-CD326 antibody (EpCAM, Miltenyi biotec), followed by staining with Alexa488- and Alexa647-conjugated secondary antibodies (Invitrogen). Hoechst 33342 was used for nuclear staining. The stained tissue samples were observed using a LSM510 META laser confocal microscope (Carl Zeiss, Germany).

3. Results

3.1. In vitro characterization of DACHPt-loaded micelles (DACHPt/m)

The polymer-metal complex formation between DACHPt and the carboxylic group of the P(Glu) in the PEG-*b*-P(Glu) led to the formation of polymeric micelles with an average diameters of approximately 30-nm (Fig. 1 and Supplementary Fig. SlA). DACHPt/m can release cytotoxic DACHPt complexes from the micelle core by the ligand

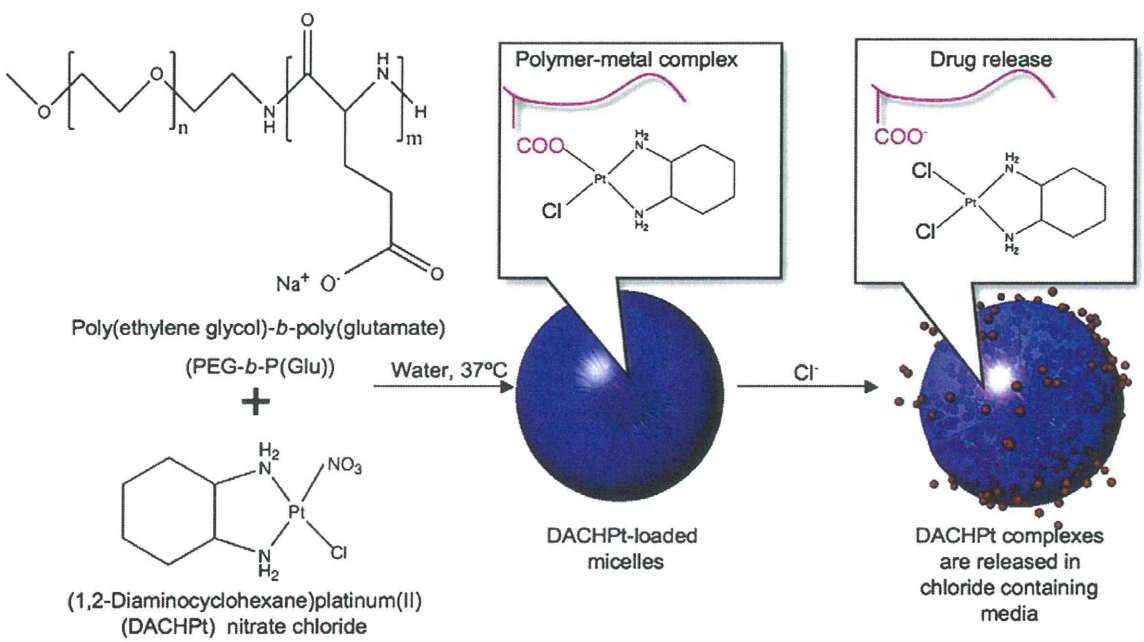

Fig. 1. Scheme of the preparation of DACHPt-loaded micelles (DACHPt/m). The micelles are formed by the polymer–metal complex formation between DACHPt and the carboxylic acid moieties in the poly(glutamic acid) backbone. DACHPt is released in a sustained manner as a result of the ligand substitution of the Pt(II) from the carboxylates in the core of the micelles with the chloride ions in the medium.

Please cite this article as: M. Rafi, et al., Polymeric micelles incorporating (1,2-diaminocyclohexane)platinum (II) suppress the growth of orthotopic scirrhous gastric tumors ..., J. Control. Release (2012), doi:10.1016/j.jconrel.2012.01.038

Table 1
Fifty-percent cell growth inhibitory concentration (IC_{50}) of DACHPt/m and oxaliplatin against human scirrhous gastric cancer OCUM-2-MLN cells.

Drug	IC_{50} (μM)	
	48 h	72 h
DACHPt/m	20.0	12.5
Oxaliplatin	12.5	6.25

exchange of DACHPt from the carboxylic groups of p(Glu) to the chloride ions in the media [28]. The 50% cell growth inhibitory concentration (IC_{50}) of DACHPt/m was approximately 2-fold higher than that of oxaliplatin (Table 1).

3.2. Antitumor activity against bioluminescent orthotopic gastric tumors

OCUM-2MLN cells stably expressing luciferase gene (OCUM-2MLN-Luc) were prepared by the lentiviral transfection. The bioluminescent signal of OCUM-2MLN-Luc after the addition of luciferin was measured by IVIS (Supplementary Fig. S2). As the light glowing from the cells increased linearly with cell density (Supplementary Fig. S2), we can use the light intensity of OCUM-2MLN-Luc to quantify the tumor burden.

The antitumor activity of oxaliplatin and DACHPt/m was studied in mice bearing orthotopic OCUM-2MLN-Luc tumors that have already developed metastasis to the lymph nodes. The mice were treated intravenously 3 times at 0, 2 and 4 days with oxaliplatin at 8 mg/kg or DACHPt/m at 4 mg/kg on a Pt basis. The photon flux (photons per second) from the bioluminescent tumors was assessed by IVIS every second day. Consequently, oxaliplatin failed to show any antitumor effect against the OCUM-2MLN-Luc tumors as the photon flux of oxaliplatin-treated mice was comparable to that of untreated mice (Fig. 2A). In contrast, the mice treated with DACHPt/m showed significantly lower relative photon flux compared with untreated and oxaliplatin-treated mice (Fig. 2A) without significant body weight loss (Fig. 2B), indicating a significant antitumor activity against the orthotopic gastric tumors.

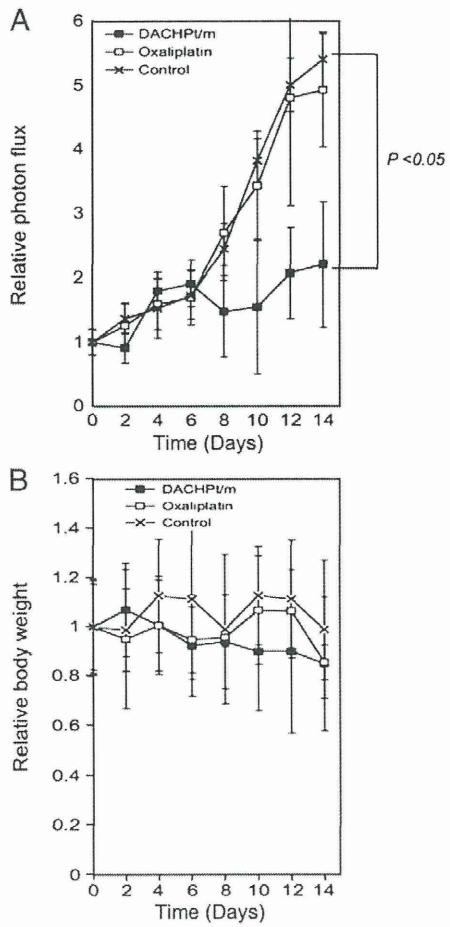

Fig. 2. Antitumor activity of oxaliplatin and DACHPt/m against bioluminescent OCUM-2-MLN-Luc orthotopic gastric cancer. A, Relative photon flux from the tumors after the injection of saline, oxaliplatin 8 mg/kg and DACHPt/m 4 mg/kg on days 0, 2 and 4. B, Relative body weight of the mice. Data are expressed as a mean ± SE ($n = 5$).

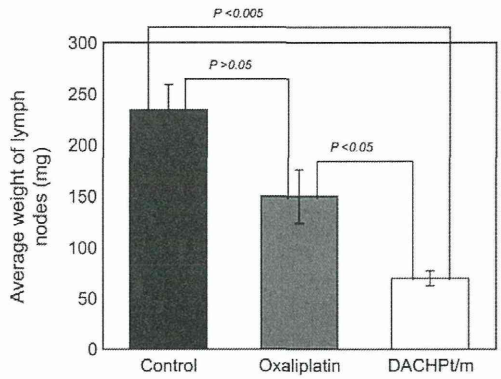

Fig. 3. Weight of the metastatic lymph nodes at the end of the antitumor activity experiment (day 14). Data are expressed as a mean ± SE ($n = 5$).

3.3. Growth inhibition of lymph node metastasis

At the end of the antitumor activity study, the mice were sacrificed and the metastatic lymph nodes were collected and weighed. As shown in Fig. 3, the weights of the lymph nodes in DACHPt/m-treated mice were approximately four and two times lower than those in untreated mice and oxaliplatin-treated mice, respectively, suggesting that DACHPt/m might effectively inhibit the growth of the metastatic lymph nodes and their efficacy might surpass that of oxaliplatin.

3.4. Biodistribution of DACHPt/m in orthotopic gastric tumors and metastatic lymph nodes

DACHPt/m gradually accumulated in the orthotopic tumors due to the EPR effect, achieving approximately 10% of injected dose per gram of tumor tissue at 24 h (Fig. 4A). The tumor accumulation at 24 h for DACHPt/m was 6 times higher than oxaliplatin (Fig. 4A). DACHPt/m also showed enhanced accumulation in sentinel and distant metastatic lymph nodes (Fig. 4B and C). The effective accumulation of DACHPt/m in the metastatic lymph nodes may account for their effective growth inhibition of lymphatic metastasis.

The *in vivo* distribution of fluorescent-labeled DACHPt/m was assessed by fluorescent imaging of the whole body of tumor-bearing mice. Twenty-four hours after intravenous injection of fluorescent-labeled DACHPt/m, intense fluorescence signal was detected at the tumor site, suggesting the selective accumulation of DACHPt/m in the orthotopic tumors (Fig. 5A). In addition, mice were sacrificed and the tumor, metastatic lymph nodes and organs (i.e., spleen, liver and kidneys) were imaged *ex vivo* (Fig. 5B). The high fluorescence signal of the micelles in the tumor and metastatic lymph nodes indicates the ability of the micelles to target the scirrhous gastric tumors and their lymphatic metastases.

Please cite this article as: M. Rafi, et al., Polymeric micelles incorporating (1,2-diaminocyclohexane)platinum (II) suppress the growth of orthotopic scirrhous gastric tumors ..., J. Control. Release (2012), doi:10.1016/j.jconrel.2012.01.038

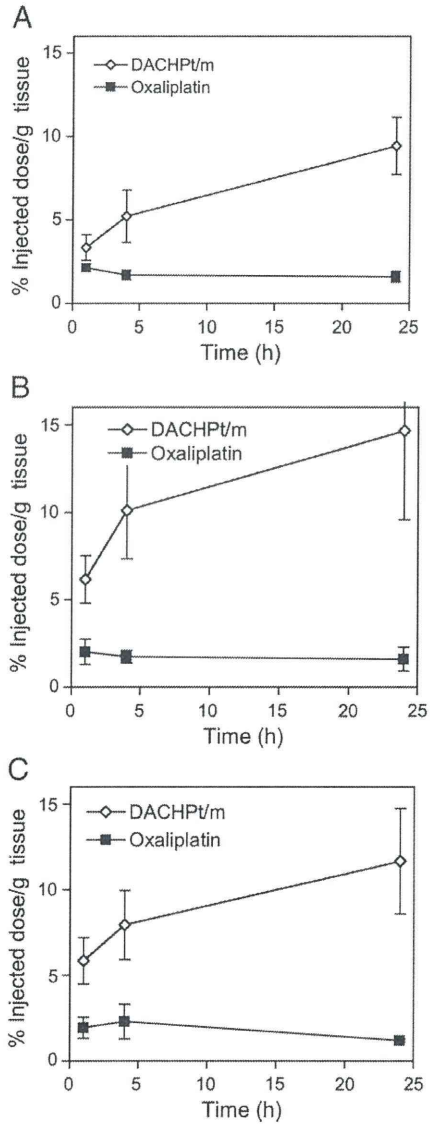

Fig. 4. Accumulation of oxaliplatin and DACHPt/m in OCUM-2-MLN-Luc orthotopic tumors and lymph node metastasis. A, Orthotopic tumor. B, Primary metastatic lymph node (sentinel lymph node). C, Secondary metastatic lymph node. Data are expressed as a mean ± SE ($n = 5$).

3.5. Microdistribution of fluorescent-labeled DACHPt/m in orthotopic tumors and metastastic lymph nodes

Firstly, the histology of OCUM-2MLN tumors was examined by H&E staining (Fig. 6A). These tumors present poorly differentiated characteristics with hypovascularity and extensive stromal fibrosis of gastric cancers [9]. The microdistribution of the fluorescent-labeled DACHPt/m in the tissue sections of the orthotopic gastric tumors was assessed by fluorescence microscopy. The nucleus of the cells in the whole tissue sections were stained with Hoechst (Fig. 6B, blue) while the tumors regions were stained by using anti-CD326 antibody (Fig. 6B, green), which recognizes the human epithelial antigen (HEA). The colocalization of the fluorescent-labeled DACHPt/m (Fig. 6B, magenta) with the CD326-stained cancer cells (Fig. 6B, green) suggests the homogeneous accumulation of the micelles in the tumor tissue (Fig. 6B). Moreover, the blood vessels, marked with anti-PECAM-1 antibody, were not detectable within the tumor (Fig. 6C, green), suggesting the hypovascular nature of the tumors. Also, the lymphatic vessels, marked with anti-LIVE-1 antibody, were not detected inside the tumor tissue (Fig. 6C, blue). In OCUM-2MLN tumor model, the cancer cells exhibit tumor invasion into peritumoral lymphatic vessels and spread along the lymphatic vessels in the gastric wall to the regional lymph nodes [33]. The fluorescence of the micelles was detected in the tumor sections even at the regions distant from the blood vessels (Fig. 6C, magenta), suggesting the deep penetration of DACHPt/m within the tumor tissue.

The H&E staining of the metastatic lymph nodes (Fig. 7A) indicated the abnormal anatomy of the lymph node due to the tumor growth. Fluorescent signal from the micelles was found to be colocalized with cancer cells, stained by CD326, in the metastatic lymph nodes, suggesting that micelles deeply penetrate into the metastases in the lymph nodes (Fig. 7B). Additionally, the lymphatic tissue and blood vessels were stained with anti-LYVE-1 and anti-PECAM-1 antibodies, respectively (Fig. 7C). LYVE-1-positive lymphatic tissue was mainly found in the periphery of the tumor in the lymph node (Fig. 7C, blue). Fluorescent-labeled micelles were found to accumulate within the tumoral region of the metastatic lymph nodes (Fig. 7C, magenta).

It is assumed that polymeric micelles from the circulation may reach the lymph nodes either through the lymphatic vessels or blood vessels. Meanwhile, the fluorescent micelles were not detected in healthy lymph nodes (Supplementary Fig. S4). The histological examinations of the enhanced accumulation of DACHPt/m in the metastatic lymph nodes are quite consistent with the significant growth inhibition of lymph node metastasis observed in DACHPt/m treated animals (Fig. 3).

4. Discussion

In the present study, we examined the targeting ability of DACHPt/m against the orthotopic model of scirrhous gastric cancer (SGC) from OCUM-2MLN cells, which is accompanied with very high rate of lymph node metastasis [30–31]. The metastasis to the lymph nodes is an important indicator for the staging of SGC and a determinant for the prognosis [35–36]. Here, we have successfully demonstrated that systemically administered DACHPt/m can target both orthotopic scirrhous gastric tumors and their lymphatic metastasis, achieving a remarkable inhibitory effect on their growth.

The biodistribution study revealed that the micelles significantly accumulated in the tumors and the metastatic lymph nodes (Figs. 5 and 6) while showing appreciably lower accumulation in organs or healthy lymph nodes (Fig. **5** and Fig.**S4**). The accumulation of DACHPt/m in the orthotopic OCUM-2MLN tumors might be related to the passive targeting based on the EPR effect. However, we have previously reported that doxorubicin-loaded polymeric micelles with 65-nm diameter showed poor accumulation and reduced efficacy against orthotopic OCUM-2MLN tumors [9]. Regarding such discrepancy, we assume that a relatively small size (30 nm) of DACHPt/m should be important for effective extravasation and tumor penetration in orthotopic OCUM-2MLN tumors. Recently, we have studied the size effect of DACHPt/m in subcutaneous human pancreatic adenocarcinoma BxPC3 tumors [29], which share histological characteristics with OCUM-2MLN tumors, such as sparse formation of blood vessels and very thick fibrotic stroma [30–31]. Accordingly, DACHPt/m with 30-nm diameter effectively extravasated and penetrated in the pancreatic tumors while DACHPt/m with diameter larger than 50-nm remained in the perivascular areas of the tumors [29]. Based on these observations, we preliminarily studied the size effect of DACHPt/m in an orthotopic OCUM-2MLN tumor model in this study (Supplementary Information). As shown in Supplementary Fig. **S3**, 30-nm DACHPt/m showed potent antitumor efficacy and enhanced tumor accumulation against gastric tumors, whereas 70-nm DACHPt/m failed to exhibit significant antitumor effect and showed

Please cite this article as: M. Rafi, et al., Polymeric micelles incorporating (1,2-diaminocyclohexane)platinum (II) suppress the growth of orthotopic scirrhous gastric tumors ..., J. Control. Release (2012), doi:10.1016/j.jconrel.2012.01.038

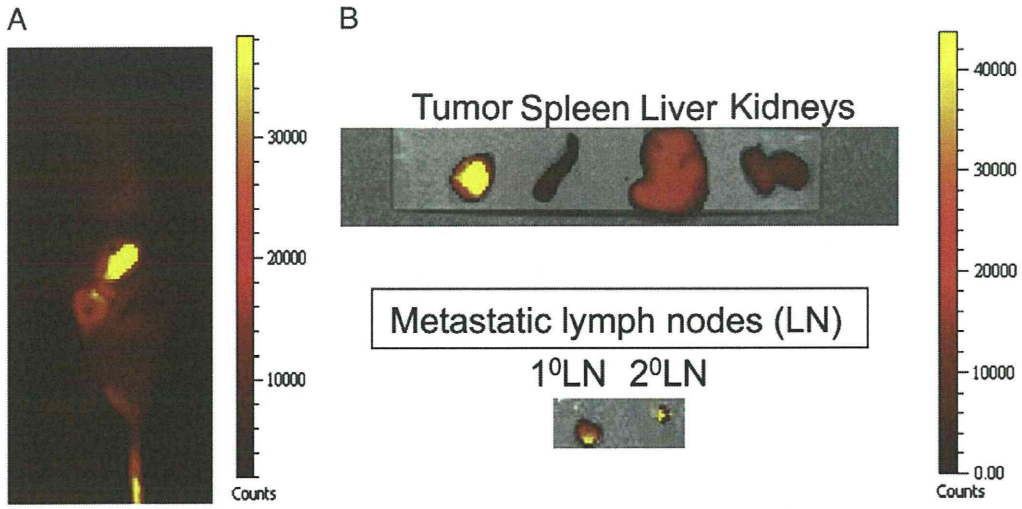

Fig. 5. Biodistribution of Alexa 680-labeled DACHPt/m. A, Whole body near infrared (NIR) fluorescent image of orthotopic OCUM-2-MLN-Luc tumor-bearing mouse 24 h after the injection of Alexa 680-labeled DACHPt/m. The micelles are detected specifically at the tumor site. B, *Ex vivo* fluorescent imaging of orthotopic tumor, organs and metastatic lymph nodes.

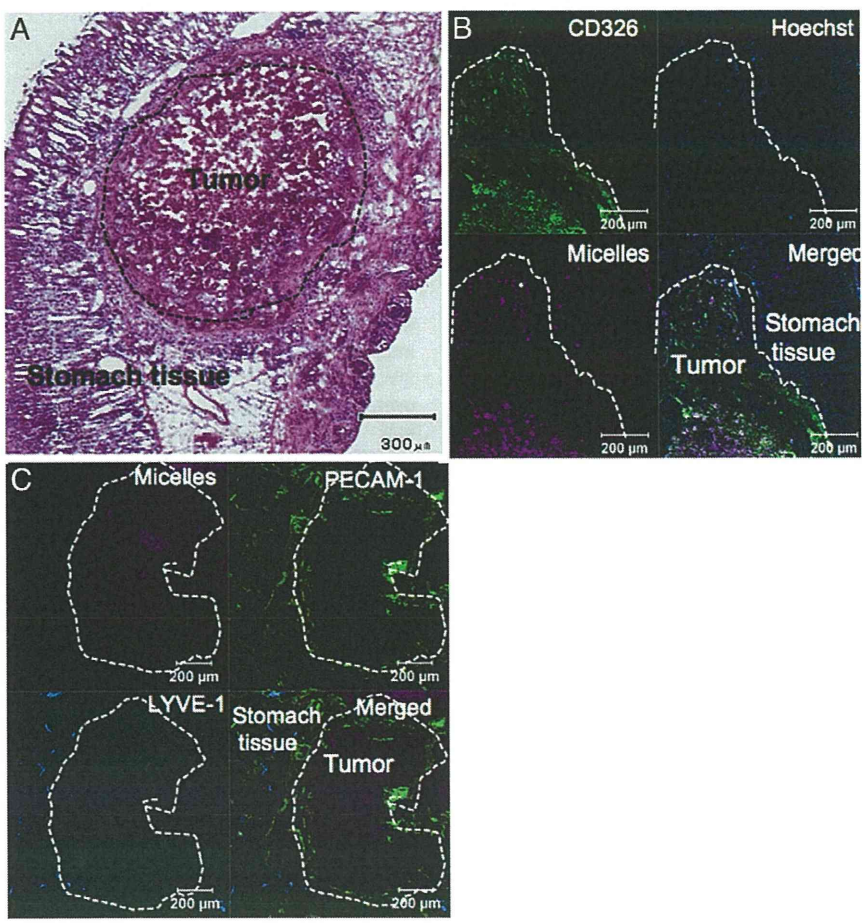

Fig. 6. Histological analysis of orthotopic OCUM-2-MLN-Luc and microdistribution of fluorescent labeled DACHPt/m. A, H&E staining of orthotopic OCUM-2-MLN-Luc tumor sections. B, Immunofluorescence microscopy of gastric cancer cells (CD326, green) and Alexa 594-labeled DACHPt/m (magenta) in orthotopic OCUM-2-MLN-Luc tumors. The cells nuclei were stained with Hoechst 33342 (blue). C, Microdistribution of Alexa 594-labeled DACHPt/m (micelles, magenta), blood vessels (PECAM-1, green) and lymphatic vessels (LYVE-1, blue) in orthotopic OCUM-2-MLN-Luc tumors determined by immunofluorescence microscopy.

Please cite this article as: M. Rafi, et al., Polymeric micelles incorporating (1,2-diaminocyclohexane)platinum (II) suppress the growth of orthotopic scirrhous gastric tumors ..., J. Control. Release (2012), doi:10.1016/j.jconrel.2012.01.038

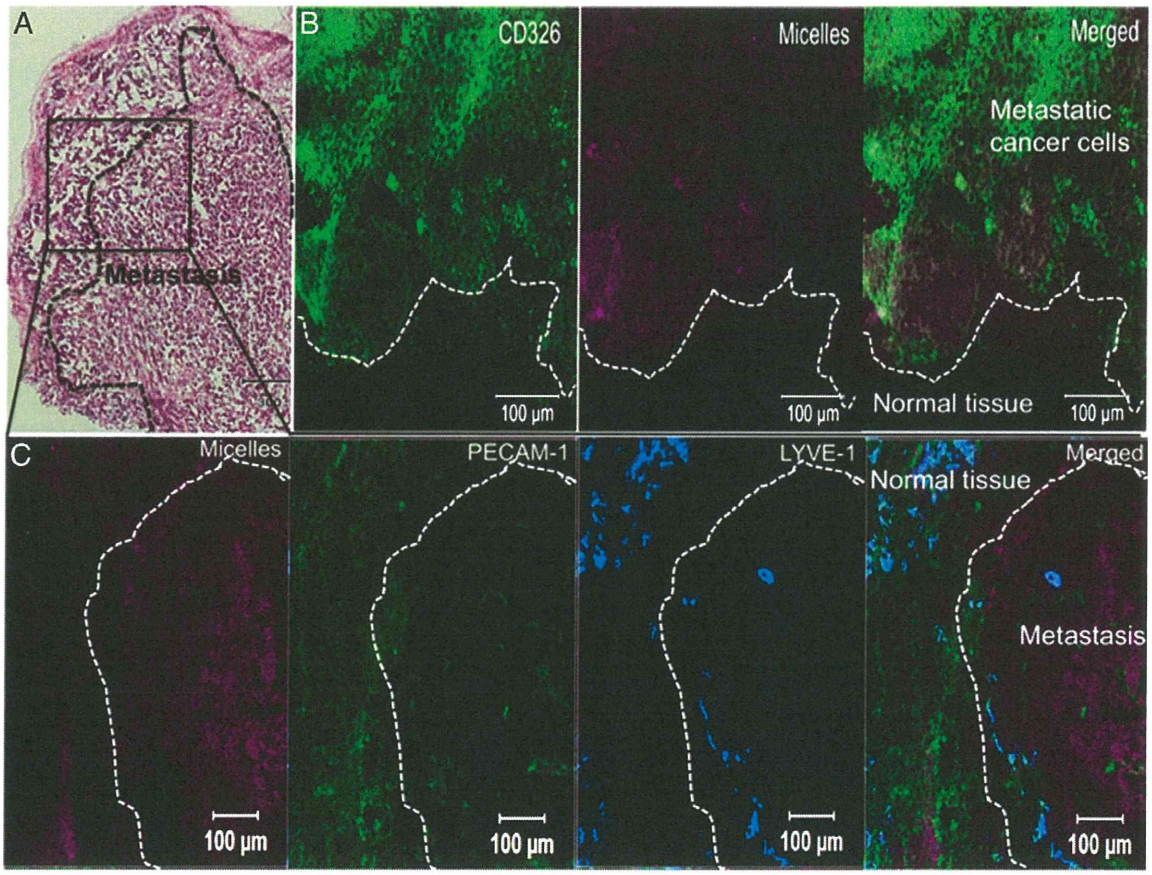

Fig. 7. Histological analysis of metastatic lymph nodes and microdistribution of fluorescent labeled DACHPt/m. A, H&E staining of metastatic lymph node. B, Immunofluorescence microscopy of gastric cancer cells (CD326, green) and Alexa 594-labeled DACHPt/m (micelles, magenta) in the metastatic lymph nodes. C, Microdistribution of Alexa 594-DACHPt/m (micelles, magenta), blood vessels (PECAM-1, green) and lymphatic vessels (LYVE-1, blue) in metastatic lymph nodes (Inset of A) determined by immunofluorescence microscopy.

poor tumor accumulation. These results are consistent with the aforementioned assumption that effective properties of DACHPt/m against a scirrhous gastric cancer model may be attributed to their relatively small size.

The observation of DACHPt/m accumulation into the fibrous OCUM-2MLN tumor here is apparently consistent with the scheme of EPR effect. On the other hand, the mechanisms of the accumulation of the micelles in the metastatic lymph nodes remain to be clarified yet. Two mechanisms for the accumulation of the micelles in the metastatic lymph nodes may be proposed: (i) the micelles accumulate in the orthotopic tumors, followed by migration and accumulation in the metastatic lymph nodes via the lymphatic vessels, (ii) the micelles can directly accumulate in the metastatic lymph nodes via blood vessels in the metastatic niche probably due to the enhanced permeability of these blood vessels. Regarding the former mechanism, intratumorally-injected nanocarriers have been demonstrated to accumulate in the metastatic lymph nodes [16,17,37,38]. Also, Harisinghani et al. reported in patients that systemically injected superparamagnetic iron oxide nanoparticles (SPION) accumulate in the metastatic lymph nodes [39]. This phenomenon was explained by accumulation of SPION in solid tumors, followed by their uptake by tumor macrophages, which migrate to metastatic lymph nodes [39]. The detailed mechanisms underlying the accumulation of the micelles in the metastatic lymph nodes are under investigation and will be reported elsewhere.

The targeting capability of the micelles to scirrhous gastric tumors and their metastatic lymph nodes could be applied not only for treatment but also for diagnosis. A variety of contrast agents, including fluorescent probes, MRI or PET contrast agents [5] can be incorporated into the micellar structure. Thus, primary scirrhous tumors and nodal involvement may be directly observed by non-invasive imaging. Moreover, the combination of therapy and imaging within single micelles may allow the evaluation of the therapeutic response, offering an emerging concept of theranostic nanomedicines [5,27].

In conclusion, our results highlight that systemically injected DACHPt/m can extravasate and penetrate in orthotopic scirrhous gastric tumors and lymph node metastasis, eliciting significantly potent antitumor activity. Enhanced drug delivery to the lymph node metastasis by polymeric micelles can improve the morbidity of the patients with SGC. DACHPt/m can also be useful for the adjuvant therapy of SGC, that is, the administration of the micelles before surgery, by improving the lymph node status while controlling the tumor volume, which may lead to the downgrading of unresectable scirrhous gastric cancer. Moreover, control of distant lymph node metastasis by DACHPt/m can impede further dissemination of the disease. Our findings suggest the high potential of systemically administered nanocarriers for the treatment of scirrhous gastric cancer as well as lymph node metastasis.

Acknowledgments

This study was supported by Funding Program for World-Leading Innovative R&D on Science and Technology (FIRST Program) from the Japan Society for the Promotion of Science (JSPS) and Grants-in-Aid

for Scientific Research from the Japanese Ministry of Health, Labour, and Welfare (MHLW).

Appendix A. Supplementary data

Supplementary data to this article can be found online at doi:10.1016/j.jconrel.2012.01.038.

References

[1] R. Duncan, The dawning era of polymer therapeutics, Nat. Rev. Drug Discov. 2 (2003) 347–360.
[2] M.E. Davis, Z. Chen, D. Shin, Nanoparticle therapeutics: an emerging treatment modality for cancer, Nat. Rev. Drug Discov. 7 (2008) 771–782.
[3] K. Kataoka, A. Harada, Y. Nagasaki, Block copolymer micelles for drug delivery: design, characterization and biological significance, Adv. Drug Deliv. Rev. 47 (2001) 113–131.
[4] N. Nishiyama, K. Kataoka, Current state, achievements, and future prospects of polymeric micelles as nanocarriers for drug and gene delivery, Pharmacol. Ther. 112 (2006) 630–648.
[5] H. Cabral, N. Nishiyama, K. Kataoka, Supramolecular nanodevices: from design validation to theranostic nanomedicine, Acc. Chem. Res. 44 (2011) 999–1008.
[6] Y. Matsumura, H. Maeda, A new concept for macromolecular therapeutics in cancer chemotherapy: mechanism of tumoritropic accumulation of proteins and the antitumor agent Smancs, Cancer Res. 46 (1986) 6387–6392.
[7] J.J. Gottlieb, K. Washenik, A. Chachoua, A. Friedman-Kien, Treatment of classic Kaposi's sarcoma with liposomal encapsulated doxorubicin, Lancet 350 (1997) 1363–1364.
[8] W.J. Gradishar, S. Tjulandin, N. Davidson, H. Shaw, N. Desai, P. Bhar, M. Hawkins, J. O'Shaughnessy, Phase III trial of nanoparticle albumin-bound paclitaxel compared with polyethylated castor oil-based paclitaxel in women with breast cancer, J. Clin. Oncol. 23 (2005) 7794–7803.
[9] M.R. Kano, Y. Bae, C. Iwata, Y. Morishita, M. Yashiro, M. Oka, T. Fujii, A. Komuro, K. Kiyono, M. Kaminishi, K. Hirakawa, Y. Ouchi, N. Nishiyama, K. Kataoka, K. Miyazono, Improvement of cancer-targeting therapy, using nanocarriers for intractable solid tumors by inhibition of TGF-β signaling, Proc. Natl. Acad. Sci. U. S. A. 104 (2007) 3460–3465.
[10] M.R. Kano, Y. Komuta, C. Iwata, M. Oka, Y.T. Shirai, Y. Morishita, Y. Ouchi, K. Kataoka, K. Miyanozo, Comparison of the effects of the kinase inhibitors imatinib, sorafenib, and transforming growth factor-β receptor inhibitor on extravasation of nanoparticles from neovasculature, Cancer Sci. 100 (2009) 173–180.
[11] K.D. Crew, A.I. Neugut, Epidemiology of gastric cancer, World J. Gastroenterol. 12 (2006) 354–362.
[12] E. Otsuji, Y. Kuriu, K. Okamoto, T. Ochiai, D. Ichikawa, A. Hagiwara, H. Yamagishi, Outcome of surgical treatment for patients with scirrhous carcinoma of the stomach, Am. J. Surg. 188 (2004) 327–332.
[13] Japanese Gastric, Cancer A Japanese classification of gastric carcinoma—2nd English Edition, Gastric Cancer 1 (1998) 10–24.
[14] Y. Hippo, M. Yashiro, M. Ishii, H. Taniguchi, S. Tsutumi, K. Hirakawa, T. Kosama, H. Aburatani, Differential gene expression profiles of scirrhous gastric cancer cells with high metastatic potential to peritoneum or lymph nodes, Cancer Res. 61 (2001) 889–895.
[15] Y. Maehara, Y. Emi, H. Baba, Y. Adachi, K. Akazawa, Y. Ichiyoshi, K. Sugimachi, Recurrences and related characteristics of gastric cancer, Br. J. Cancer 74 (1996) 975–979.
[16] A. Hagiwara, T. Takahashi, K. Sawai, C. Sakakura, M. Shirasu, M. Ohgaki, T. Imanishi, J. Yamasaki, Y. Takemoto, N. Kageyama, Selective drug delivery to peri-tumoral region and regional lymphatics by local injection of aclarubicin adsorbed on activated carbon particles in patients with breast cancer—a pilot study, Anticancer Drugs 8 (1997) 666–670.
[17] C. Oussoren, G. Storm, Liposomes to target the lymphatics by subcutaneous administration, Adv. Drug Deliv. Rev. 50 (2001) 143–156.
[18] P. Hirnle, Targeted introduction of substances into the lymph nodes for endolymphatic therapy, in: Stanley P.L. Leong (Ed.), Cancer metastasis and the lymphovascular system: basis for rational therapy, Springer, 2007, p. 101.
[19] K. Yamagata, K. Kumagai, K. Shimizu, K. Masuo, Y. Nishida, A. Yasui, Gastrointestinal cancer metastasis and lymphogenous spread: viewpoint of animal models of lymphatic obstruction, Jpn. J. Clin. Oncol. 28 (1998) 104–106.
[20] Y. Matsumura, T. Hamaguchi, T. Ura, K. Muro, Y. Yamada, Y. Shimada, K. Shirao, T. Okusaka, H. Ueno, M. Ikeda, N. Watanabe, Phase I clinical trial and pharmacokinetic evaluation of NK911, a micelle-encapsulated doxorubicin, Br. J. Cancer 91 (2004) 1775–1781.
[21] T. Hamaguchi, K. Kato, H. Yasui, C. Morizane, M. Ikeda, H. Ueno, K. Muro, Y. Yamada, T. Okusuka, K. Shirao, Y. Shimada, H. Nakahama, Y. Matsumura, A phase I and pharmacokinetic study of NK105, a paclitaxel-incorporating micellar nanoparticle formulation, Br. J. Cancer 97 (2007) 170–176.
[22] Y. Matsumura, K. Kataoka, Preclinical and clinical studies of anticancer agent-incorporating polymer micelles, Cancer Sci. 100 (2009) 572–579.
[23] Y. Matsumura, Preclinical and clinical studies of NK012, an SN-38-incorporating polymeric micelles, which is designed based on EPR effect, Adv. Drug Deliv. Rev. 63 (2010) 184–192.
[24] R. Plummer, R.H. Wilson, H. Calvert, A.V. Boddy, M. Griffin, J. Sludden, M.J. Tilby, M. Eatock, D.G. Pearson, C.J. Ottley, Y. Matsumura, K. Kataoka, T. Nishiya, A Phase I clinical study of cisplatin-incorporated polymeric micelles (NC-6004) in patients with solid tumours, Br. J. Cancer 104 (2011) 593–598.
[25] H. Cabral, N. Nishiyama, S. Okazaki, H. Koyama, K. Kataoka, Preparation and biological properties of dichloro(1,2-diaminocyclohexane)platinum (II) (DACHPt)-loaded polymeric micelles, J. Control. Release 101 (2005) 223–232.
[26] H. Cabral, N. Nishiyama, K. Kataoka, Optimization of (1,2-diamino-cyclohexane) platinum(II)-loaded polymeric micelles directed to improved tumour targeting and enhanced antitumour activity, J. Control. Release 121 (2007) 146–155.
[27] S. Kaida, H. Cabral, M. Kumagai, A. Kishimura, Y. Terada, M. Sekino, I. Aoki, N. Nishiyama, T. Tani, K. Kataoka, Visible drug delivery by supramolecular nanocarriers directing to single-platformed diagnosis and therapy of pancreatic tumor model, Cancer Res. 70 (2010) 7031–7041.
[28] M. Murakami, H. Cabral, Y. Matsumoto, S. Wu, M.R. Kano, T. Yamori, N. Nishiyama, K. Kataoka, Improving drug potency and efficacy by nanocarrier-mediated subcellular targeting, Sci. Transl. Med. 3 (2011) 64ra2.
[29] H. Cabral, Y. Matsumoto, K. Mizuno, Q. Chen, M. Murakami, M. Kimura, Y. Terada, M.R. Kano, K. Miyazono, M. Uesaka, N. Nishiyama, K. Kataoka, Accumulation of sub-100nm polymeric micelles in poorly permeable tumours depends on size, Nat. Nanotech. 6 (2011) 815–823.
[30] T. Fujihara, T. Sawada, K. Hirakawa, Y.S. Chung, M. Yashiro, T. Inoue, M. Sowa, Establishment of lymph node metastatic model for human gastric cancer in nude mice and analysis of factors associated with metastasis, Clin. Exp. Metastasis 16 (1998) 389–398.
[31] M. Yashiro, K. Hirakawa, Cancer–stromal interactions in scirrhous gastric carcinoma, Cancer Microenviron. 3 (2010) 127–135.
[32] K. Shibuya, J. Shirakawa, T. Kameyama, S. Honda, S. Tahara Hanaoka, A. Miyamoto, M. Onodera, T. Sumida, H. Nakauchi, H. Miyoshi, A. Shibuya, CD226 (DNAM-1) is involved in lymphocyte function-associated antigen 1 costimulatory signal for naive T cell differentiation and proliferation, J. Exp. Med. 198 (2003) 1829–1839.
[33] C. Iwata, M.R. Kano, A. Komuro, M. Oka, K. Kiyono, E. Johansson, Y. Morishita, M. Yashiro, K. Hirakawa, M. Kaminishi, K. Miyazono, Inhibition of cyclooxygenase-2 suppresses lymph node metastasis via reduction of lymphangiogenesis, Cancer Res. 67 (2007) 10181–10189.
[34] D.E. Jenkins, Y. Oei, Y.S. Hornig, S.F. Yu, J. Dusich, T. Purchio, P.R. Contag, Bioluminescent imaging (BLI) to improve and refine traditional murine models of tumor growth and metastasis, Clin. Exp. Metastasis. 20 (2003) 733–744.
[35] M.S. Karpeh, L. Leon, D. Klimstra, M.F. Brennan, Lymph node staging in gastric cancer: is location more important than Number? An analysis of 1,038 patients, Ann. Surg. 232 (2000) 362–371.
[36] C.Y. Chen CY, C.W. Wu, S.S. Lo, M.C. Hsieh, W.Y. Lui, K.H. Shen, Peritoneal carcinomatosis and lymph node metastasis are prognostic indicators in patients with Borrmann type IV gastric carcinoma, Hepatogastroenterology 49 (2002) 874–877.
[37] C. Oussoren, G. Storm, Lymphatic uptake and biodistribution of liposomes after subcutaneous injection: III. Influence of surface modification with poly(ethyleneglycol), Pharm. Res. 14 (1997) 1479–1484.
[38] G. Luo, X. Yu, C. Jin, F. Yang, D. Fu, J. Long, J. Xu, C. Zhan, W. Lu, LyP-1-conjugated nanoparticles for targeting drug delivery to lymphatic metastatic tumors, Int. J. Pharm. 385 (2010) 150–156.
[39] M.G. Harisinghani, J. Barentsz, P.F. Hahn, W.M. Deserno, S. Tabatabaei, C.H. van de Kaa, J. de la Rosette, R. Weissleder, Noninvasive detection of clinically occult lymph-node metastases in prostate cancer, N. Engl. J. Med. 348 (2003) 2491–2499.

nature nanotechnology

ARTICLES

PUBLISHED ONLINE: 23 OCTOBER 2011 | DOI: 10.1038/NNANO.2011.166

Accumulation of sub-100 nm polymeric micelles in poorly permeable tumours depends on size

H. Cabral[1], Y. Matsumoto[2], K. Mizuno[3], Q. Chen[4], M. Murakami[2], M. Kimura[2], Y. Terada[5], M. R. Kano[6], K. Miyazono[6,7], M. Uesaka[3,7], N. Nishiyama[2,7]* and K. Kataoka[1,2,4,7]*

A major goal in cancer research is to develop carriers that can deliver drugs effectively and without side effects. Liposomal and particulate carriers with diameters of ~100 nm have been widely used to improve the distribution and tumour accumulation of cancer drugs, but so far they have only been effective for treating highly permeable tumours. Here, we compare the accumulation and effectiveness of different sizes of long-circulating, drug-loaded polymeric micelles (with diameters of 30, 50, 70 and 100 nm) in both highly and poorly permeable tumours. All the polymer micelles penetrated highly permeable tumours in mice, but only the 30 nm micelles could penetrate poorly permeable pancreatic tumours to achieve an antitumour effect. We also showed that the penetration and efficacy of the larger micelles could be enhanced by using a transforming growth factor-β inhibitor to increase the permeability of the tumours.

Targeting tumours with long-circulating nanomedicines, such as poly(ethylene glycol)-modified liposomes and polymeric micelles[1–6], is a promising strategy in systemic cancer treatment. These materials accumulate in solid tumours through the enhanced permeability and retention (EPR) effect[7], which is characterized by leaky blood vessels and an impaired lymphatic drainage in tumour tissues[7]. Compared with free drug, nanomedicines accumulate in solid tumours more easily and selectively and therefore offer better antitumour activity[8–15]. Several nanomedicines, including Doxil and Abraxane (diameters of 90 and 130 nm, respectively), have shown significant antitumour activity in highly vascularized tumours such as Kaposi's sarcoma and breast cancer, and have been approved for clinical use[16,17]. However, because Doxil and other nanomedicines with diameters larger than 100 nm have shown limited penetration and accumulation in tumours with hypovascular and hypopermeable characteristics[18–20] (such as intractable pancreatic tumours[18,20]), nanomedicines in the sub-100 nm range are now regarded as being more important in the study of tumour penetration[21,22].

Polymeric micelles (self-assemblies of block copolymers) are promising long-circulating nanomedicines[5,6,8–10] and have been widely studied in preclinical and clinical trials[13,14,23]. Clinical studies have demonstrated that polymeric micelles of poly(ethylene glycol)–*b*-poly(amino acid) copolymers incorporating paclitaxel, SN-38, doxorubicin or cisplatin drugs can reduce the toxic side effects of the loaded drugs[13,14,24,25] while maintaining appreciable antitumour efficacy. Micelles containing paclitaxel and SN-38 have been reported to reduce the size of tumours in patients with advanced cancers of the breast and pancreas[13,14]. The dense poly(ethylene glycol) (PEG) shell of the micelles prevents protein adsorption and recognition by the phagocyte system, and this prolongs blood circulation, a prerequisite for enhanced tumour accumulation based on the EPR effect. Moreover, with these micelles, the size (including those in the sub-100 nm range), stability, loading capacity and release kinetics of the drugs can be modulated by engineering the constituent block copolymers[5,6]. Here, we examine whether a series of micellar nanomedicines that have diameters less than 100 nm and that carry the potent tumoricidal agent 1,2-diaminocyclohexane-platinum(II) (DACHPt) (the parent complex of oxaliplatin) can accumulate and penetrate poorly permeable pancreatic tumours. Our results show that the size of the nanomedicines critically affects the penetration and efficacy of the drugs in the tumours. Larger micelles that could not penetrate otherwise, could penetrate once the permeability of the tumours was improved by administering a transforming growth factor-β inhibitor.

Characterization of DACHPt-loaded micelles

DACHPt-loaded micelles (DACHPt/m) were spontaneously formed from the interaction of the platinum of DACHPt and the carboxylic moieties of PEG–*b*-poly(glutamic acid) (PEG–*b*-P(Glu)) copolymer and the poly(glutamic acid) (P(Glu)) homopolymer in water (Fig. 1a)[10,26,27]. Differently sized DACHPt/m were synthesized by controlling the mixing ratio of P(Glu) from the homopolymer and the P(Glu) portion of PEG–*b*-P(Glu) (Fig. 1b). As the ratio of P(Glu) in the homopolymer and P(Glu) in the copolymer increases, the size of the micelles increases. Thus, the size of DACHPt/m ranged from 30 nm without the addition of P(Glu) homopolymer to more than 100 nm, while maintaining a narrow distribution as determined by dynamic light scattering (DLS) measurements and transmission electron microscopy (TEM) observations (Table 1 and Supplementary Fig. S1, respectively). Note that DLS measurements provide the hydrodynamic diameter of the DACHPt/m, and TEM gives the core diameter of the micelles, so the difference between the hydrodynamic diameter and the core size gives an indication of the thickness of the PEG shell of the micelles.

[1]Department of Bioengineering, Graduate School of Engineering, The University of Tokyo, 7-3-1 Hongo, Bunkyo-ku, Tokyo, 113-8656, Japan, [2]Center for Disease Biology and Integrative Medicine, Graduate School of Medicine, The University of Tokyo, 7-3-1 Hongo, Bunkyo-ku, Tokyo 113-0033, Japan, [3]Department of Nuclear Engineering and Management, Graduate School of Engineering, The University of Tokyo, 7-3-1 Hongo, Bunkyo-ku, Tokyo 113-8656, Japan, [4]Department of Materials Engineering, Graduate School of Engineering, The University of Tokyo, 7-3-1 Hongo, Bunkyo-ku, Tokyo 113-8656, Japan, [5]SPring 8, JASRI, 1-1-1 Kouto, Sayo-cho, Sayo-gun, Hyogo 679-5198, Japan, [6]Department of Molecular Pathology, Graduate School of Medicine, The University of Tokyo, 7-3-1 Hongo, Bunkyo-ku, Tokyo 113-0033, Japan, [7]Center for NanoBio Integration (CNBI), The University of Tokyo, 7-3-1 Hongo, Bunkyo-ku, Tokyo 113-8656, Japan. *e-mail: nishiyama@bmw.t.u-tokyo.ac.jp; kataoka@bmw.t.u-tokyo.ac.jp

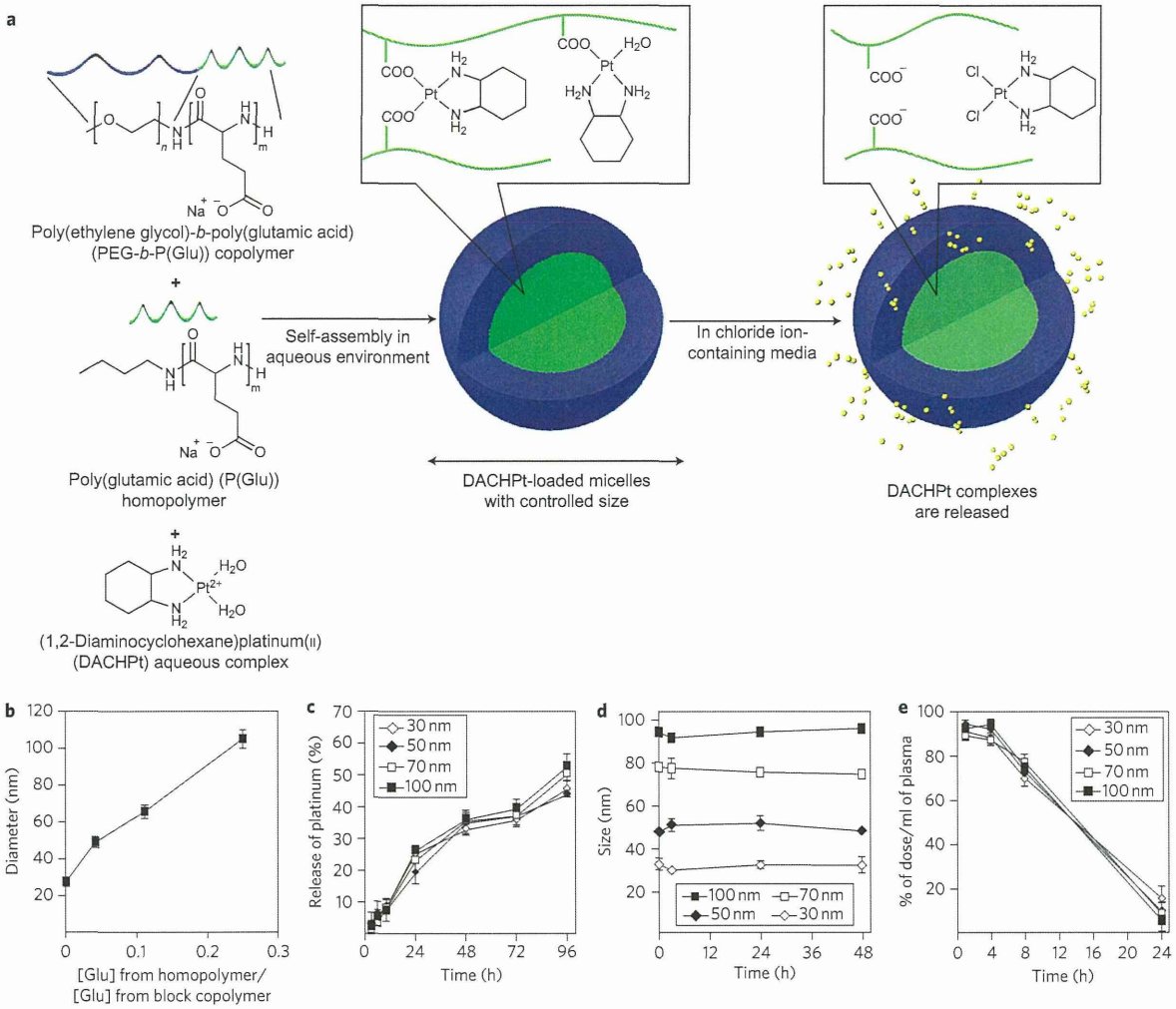

Figure 1 | Construction and physicochemical properties of DACHPt-loaded micellar nanomedicines (DACHPt/m) with different diameters. a, Schematic showing DACHPt/m formed through the interaction between DACHPt and the carboxylic groups of poly(glutamic acid) (green) in PEG-*b*-P(Glu) and P(Glu). In media containing chloride ions, DACHPt (yellow circles) is released from the micelles through ligand exchange between the carboxylic groups in P(Glu) and the chloride ions. **b**, Changing micelle size by altering the ratio of P(Glu) from the homopolymer and the P(Glu) portion of PEG-*b*-P(Glu) in the mixture. Total glutamic acid residue concentration was maintained at 5 mM. **c**, Micelles of all sizes release DACHPt at similar rates. **d**, Micelles of all sizes incubated in cell culture media containing 10% serum at 37 °C maintained their sizes over 48 h. **e**, Plasma clearances of micelles with different diameters follow similar trends. Data are means ± s.e.m., $n = 3$.

Table 1 | Diameter, size distribution, drug loading and surface charge of 30, 50, 70 and 100 nm micelles.

Size (nm)*	Polydispersity index	[Pt]/[COO] (mol/mol)†	Pt/polymer (wt/wt%)	Zeta-potential (mV)‡
30	0.16	0.56	34	−2.29 ± 1.41
54	0.14	0.6	48	−1.61 ± 0.58
69	0.12	0.57	54	−0.89 ± 0.33
110	0.11	0.52	69	0.15 ± 0.21

*Determined by DLS. †Determined by ICP-MS (platinum concentration) and weight of micelles. ‡Determined by laser doppler electrophoresis ($n = 4$, mean ± s.d.).

The 30, 50, 70 and 100 nm DACHPt/m presented similar zeta potentials, ranging from −2.29 to 0.15 mV at pH 7.4 (Table 1). These micelles showed similar drug release rates (Fig. 1c), driven by the ligand exchange of DACHPt between the carboxylic groups of P(Glu) and the chloride ions in the biological media. After 96 h incubation in cell culture media containing 10% fetal bovine serum (FBS) at 37 °C, the drug release from DACHPt/m reached ~50% (Fig. 1c). Under similar conditions, differently sized DACHPt/m maintained their diameters for over 48 h (Fig. 1d). DACHPt/m of different sizes also showed similar plasma clearance rates (~12% of injected dose (ID) per ml plasma remained after 24 h) and plasma half-lives (7–8 h) (Fig. 1e and Supplementary Table S1, respectively). We recently showed that DACHPt/m can maintain their micellar structure in the circulation for at least 24 h after injection[28]. Furthermore, DACHPt/m of varying sizes show similar distributions in the kidney, liver and spleen (Supplementary Fig. S2 and

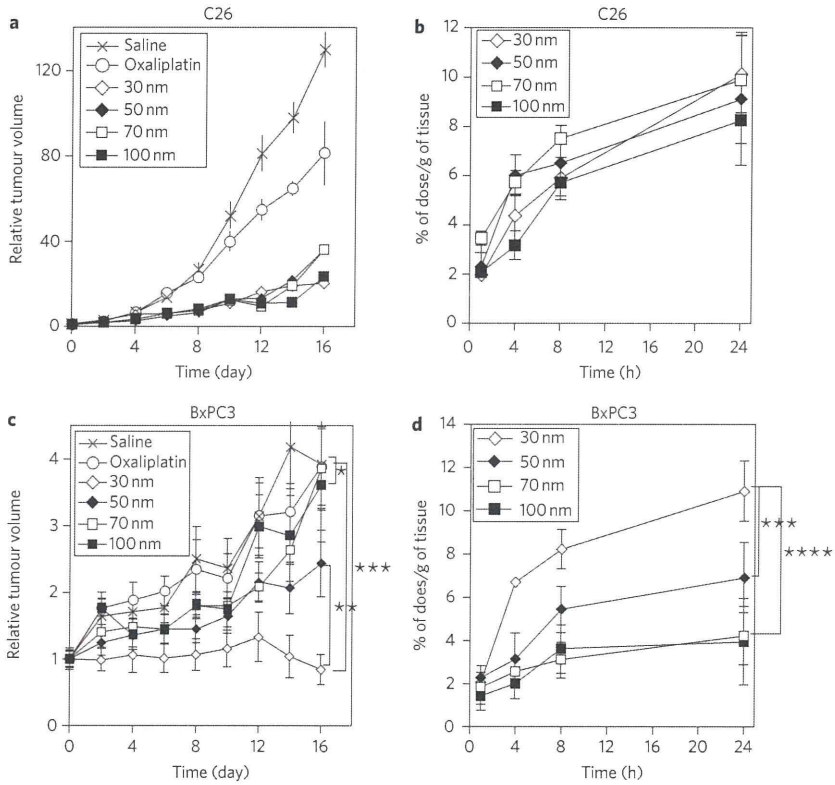

Figure 2 | Anticancer activity and tumour accumulation of DACHPt/m with different diameters. a–d, Plots of relative tumour volumes of subcutaneous hyperpermeable murine colon adenocarcinoma (C26) (**a**) and subcutaneous hypopermeable human pancreatic adenocarcinoma BxPC3 (**c**) tumours, and accumulation of DACHPt/m in C26 (**b**) and BxPC3 (**d**) tumours. To evaluate antitumour activity, oxaliplatin was injected on days 0, 2 and 4 (dose, 8 mg kg^{-1}) and micelles were injected on days 0, 2 and 4 (dose, 3 mg kg^{-1} on a platinum basis). For tumour accumulation experiments, micelles were injected at 100 μg per mouse on a platinum basis. Data are means ± s.e.m., $n = 6$. *$P > 0.05$; **$P < 0.05$; ***$P < 0.01$; ****$P < 0.001$.

Table S1), which are the major organs responsible for the clearance of nanocarriers[29]. The levels of accumulation of DACHPt/m in these organs are comparable to other polymeric micelles incorporating cisplatin[8] or doxorubicin[9], except for a slightly higher accumulation of 100 nm DACHPt/m in the liver. Because the surface chemistry and charge of nanocarriers have been reported to critically affect the interactions of nanocarriers with plasma proteins and cells and the biodistributions of nanocarriers[21,22,29,30], the analogous surface chemistry (PEG-coated surface), neutral charge and comparable plasma clearance of DACHPt/m with different diameters are substantial advantages for the evaluation of their extravasation, penetration and accumulation abilities in solid tumours as well as the associated therapeutic outcomes.

Antitumour activity of DACHPt/m in solid tumours

The antitumour activity and accumulation of DACHPt/m with different diameters were examined in tumour models with different permeabilities: a hyperpermeable murine colon adenocarcinoma 26 (C26) model characterized by high vascularization and slight tumour stroma[31] and a human pancreatic adenocarcinoma BxPC3 characterized by low vascularization, reduced vascular permeability due to pericyte coverage of blood vessels[20,31] and thick fibrosis, which are representative characteristics of some intractable solid tumours[20,31–33]. Note that the *in vitro* cytotoxicity of sub-100 nm DACHPt/m on C26 and BxPC3 cell lines was not substantially affected by micelle size (Supplementary Table S3), suggesting that their *in vivo* antitumour effect can be associated with their accumulation and microdistribution in solid tumours. In the C26 model, all micelles demonstrated comparable tumour growth inhibition (Fig. 2a), whereas oxaliplatin did not show a significant antitumour effect. The accumulation levels of all sub-100 nm micelles in C26 tumours were consistently comparable, reaching ~10% ID g^{-1} tumour at 24 h post-injection (Fig. 2b). In the BxPC3 model, the size effect of DACHPt/m on antitumour activity became evident, with the 30 nm micelles completely suppressing tumour growth, the 50 nm micelles leading to reduced antitumour activity, and the 70 nm and 100 nm micelles failing to show any antitumour effect (Fig. 2c). The accumulation of the 30 nm micelles was two times higher than that of the 50 nm micelles and four times higher than that of the 70 and 100 nm micelles after 24 h in BxPC3 tumours (Fig. 2d), which is also consistent with the antitumour efficacies in Fig. 2c.

The intratumoral microdistribution of fluorescently labelled DACHPt/m with different sizes in tumour sections was studied to investigate size-dependent extravasation and penetration of micellar nanomedicines in tumours. Histological investigations using haematoxilyn and eosin (H&E) staining revealed a well-vascularized medullary histological pattern of C26 tumours with reduced tumour stroma (Fig. 3a). In this tumour model, the fluorescence signals from the 30, 50, 70 and 100 nm micelles were uniformly distributed throughout the entire section at 24 h post-injection, suggesting deep tumour penetration of all sub-100 nm micelles (Fig. 3b, red). The immunofluorescence localization of platelet endothelial cell adhesion molecule-1 (PECAM-1), expressed by endothelial cells, indicated the extensive distribution of blood vessels in C26 tumours (Fig. 3b, green). However, H&E staining of BxPC3 tumours revealed the formation of nests of cancer cells surrounded by fibrotic tissue (Fig. 3c), which may act as a barrier

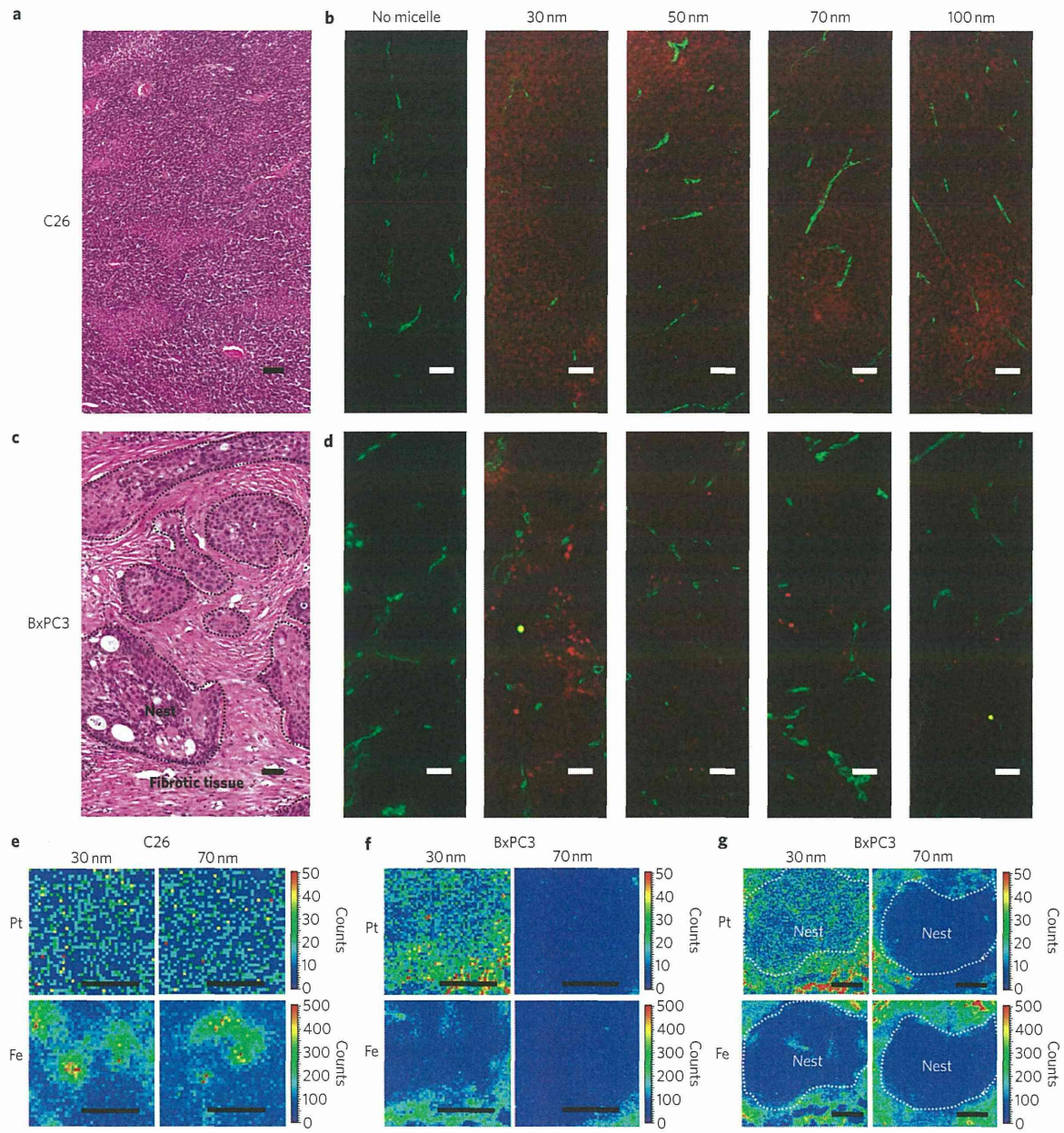

Figure 3 | Microdistribution of fluorescently labelled DACHPt/m of varying sizes in tumours. a–d, Histological examination of C26 tumour (**a**) and BxPC3 tumour (**c**) by H&E staining (dashed lines in **c** show area of cancer cell nests in the BxPC3 tumour) and fluorescent microscopic images of sections of C26 (**b**) and BxPC3 (**d**) tumours 24 h after intravenous administration of fluorescent micelles with different sizes. Micelles were labelled with Alexa 594 (red). Blood vessels were marked with PECAM-1 and Alexa 488 secondary antibody (green). Scale bars, 50 μm. **e–g**, Mapping of platinum atoms from DACHPt and iron from haemoproteins in tumour sections of C26 (**e**), BxPC3 (**f**) and a BxPC3 cancer cell nest (indicated by dashed line) (**g**) by μ-SR-XRF 24 h after administration of micelles. Scale bars, 50 μm.

against the penetration of drugs and nanocarriers[20,31]. In the BxPC3 model, immunofluorescence detection of PECAM-1 (Fig. 3d, green) indicated the presence of blood vessels around the cancer cell nests and the absence of vessels in the interior of these structures. We observed that the 30 nm micelles penetrated inside the tightly nested structures of BxPC3 tumours, but the fluorescent signal of the bigger micelles diminished and was concentrated close to the blood vessels, indicating their failure to enter the nests of cancer cells (Fig. 3d, red). This size-dependent penetration of fluorescent DACHPt/m may affect the intratumoral distribution of the delivered drug.

Given that the drug loaded in the micelles was a platinum complex, we assessed the drug microdistribution in tumour sections by detecting element disposition using μ-synchrotron radiation X-ray fluorescence (μ-SR-XRF). The very distinct peak of the platinum from the DACHPt can be observed in the sum spectrum of the line scan as well as the elements traditionally present in animal tissue. The distribution of iron and platinum in tumour tissue